CHAPTER - 5

DIELECTRIC RELAXATION OF Fe_2O_3/Gd_2O_3 CORE-SHELL NANOPARTICLES

5.1 Introduction

Development of high dielectric constant nanomaterials has been a major challenge of integral capacitor technology. High dielectric constant nanoparticles (NPs) are being continuously explored by the researchers in response to the need for power-ground decoupling to secure integrity of high-speed signals with the reduced electromagnetic interference radiated noise [1-3]. Recently, core-shell nanoparticles (CSNPs) containing metal oxides have attracted a great deal of interest from researchers because they frequently exhibit unexpected hybrid properties synergistically derived from both components [4-7]. The control and design of characteristic structural features on the nanometer scale impart them with tailored properties for diverse applications. Thus, CSNPs have been extensively studied since they exhibit interesting properties with many applications such as biomedical [8] and pharmaceutical applications [9], catalysis [10], electronics [11], enhancing photoluminescence [12] and creating photonic crystals [13]. CSNPs are highly functional materials with modified properties. Sometimes properties arising from either core or shell materials can be quite different. The properties can be modified by changing either the constituting materials or the core to shell ratio [14]. Because of the shell material coating, the properties of the core particle (such as reactivity) decrease or thermal stability can be modified, so that the overall particle stability of the core particle increases. Ultimately, particles show distinctive properties of the different materials employed together. This is especially true of the inherent ability to manipulate the surface functions to meet the diverse application requirements [9, 10]. Dielectric properties of the CSNPs have been investigated by many groups and they

reported core-shell structure enhanced the dielectric constant value compared to their single counterpart [15-17]. Zhang *et al*. [18] have observed the multipolarization phenomena in Co/graphite composites with the core/shell architecture. Lin *et al*. [19] have found the high permeability and large dielectric constant in nickel oxide (NiO) based CSNPs.

Iron oxides (Fe_2O_3) are important materials for many industrial applications such as pigments, magnetic materials, catalysts and sensors [20-23]. The dielectric properties of iron oxide have been investigated and it has been observed that they exhibit high dielectric constant and low loss at the nanoscale [24, 25]. Gadolinium oxide (Gd_2O_3) in its crystalline and amorphous phases has been of research interest as a replacement gate oxide material for silicon dioxide because of its high dielectric constant ~14 [26]. Nanocrystals (NCs) of Gd_2O_3 have been investigated for their applications as a magnetic contrast agents [27] and host materials in light emitting materials [28]. Recently, dielectric studies of amorphous Gd_2O_3 films embedded with Gd_2O_3 NCs has revealed intriguing charge storage characteristics of the NCs [29].

In the present work, Gd_2O_3 is used as coating material over the Fe_2O_3 NPs to prevent the agglomeration. The dielectric relaxation of the synthesised Fe_2O_3/Gd_2O_3 CSNPs have been investigated in a wide temperature and frequency range using alternating current impedance spectroscopy (AICS).

5.2 Experimental Procedure

The reagent grade of $Gd(NO_3)_3.6H_2O$(Alfa Aesar) and $FeCl_3$ (Merck) were used as starting materials and polyethylene glycol 400 (PEG) was used as solvent. We have used the chemical method to synthesise Fe_2O_3 core followed by nucleation and growth of Gd_2O_3 shell on the core particles.

For the synthesis of Fe_2O_3, 12mM of $FeCl_3$ was dissolved in 30 ml of PEG under stirring at 100 $^{\circ}$C. The clear transparent yellowish salt solution was subsequently heated to 180 $^{\circ}$C for 90 min. The resulting reddish brown solution of Fe_2O_3 was cooled down to room temperature, diluted with ethanol and the NPs of Fe_2O_3 were separated from the solution by centrifugation at 10,000 rpm. For the synthesis of Gd_2O_3 NPs, 12 mM of $Gd(NO_3)_3.6H_2O$ was dissolved in 30 ml of PEG under stirring at 100 $^{\circ}$C, subsequently heated to 180 $^{\circ}$C for 90 min and finally cooled down to room temperature. The brown suspension of Gd_2O_3 was diluted with ethanol and the NPs were separated from the solutions by centrifugation at 10,000 rpm. To remove any unreacted precursor and PEG, the sediment materials were dispersed in ethanol and centrifuged at several times. The materials obtained after centrifugation were calcined at 600 $^{\circ}$C for 2 h in air.

To get the NPs of Fe_2O_3/Gd_2O_3 core/shell, Gd_2O_3 shell was grown on the Fe_2O_3 core employing a two step process. Firstly, the as-prepared Fe_2O_3 core NPs were dispersed in 25 ml of PEG under sonication for 10 min and then a solution of PEG (15 ml) containing 12 mM of $Gd(NO_3)_3.6H_2O$ was injected into the dispersed nanocore system. After mixing the above solution (using a magnetic stirrer for 15 min), the mixed system was heated at 180 $^{\circ}$C for 2 h, and cooled down to room temperature, washed, centrifuged and after that calcined at 600 $^{\circ}$C for 2 h in air to get Fe_2O_3/Gd_2O_3 CSNPs. The phase purity and crystal structure of the synthesised samples were analysed by powder X-ray diffractometer (Rigaku Miniflex-II) at room temperature. The micro-structural investigation of the CSNPs was done using transmission electron microscope (TEM) (TECHNAI G^2 TF20ST) operating at 200 kV. Samples for TEM were prepared by placing a drop of colloidal acetone solution of the powder sample onto a carbon coated Cu grid and the grid was dried in air. The impedance, phase factor, capacitance and conductance of the samples were measured

using an LCR meter (HIOKI) in the frequency range from 42 Hz to 1.1 MHz at the oscillation voltage of 1.0 V. The measurements were performed over the temperature range from room temperature (303 K) to 553 K using an inbuilt cooling-heating system. Each measured temperature was kept constant with an accuracy of ±1 K. The complex electric modulus M* (= 1/ε*) and the ac electrical conductivity σ (= $\omega\varepsilon_o$ ε'') were obtained from the temperature dependence of the real (ε') and imaginary (ε'') components of the complex dielectric constant ε* (= ε' - jε'').

5.3 Results and Discussion

5.3.1 X-ray Diffraction Studies

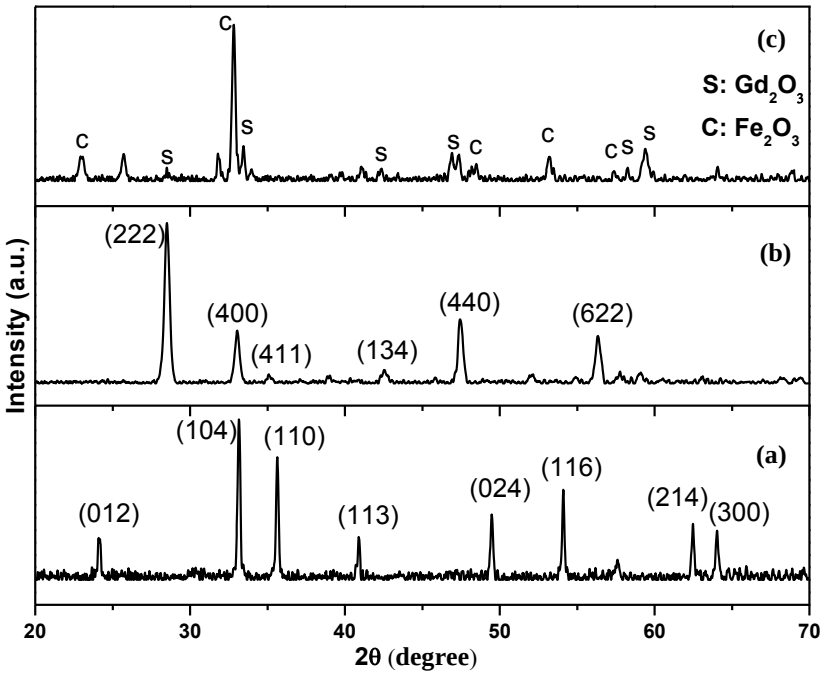

Figure 5.1 X-ray diffraction patterns of (a) Fe_2O_3, (b) Gd_2O_3 and (c) Fe_2O_3/Gd_2O_3 NPs

The XRD patterns of Fe_2O_3, Gd_2O_3 and Fe_2O_3/Gd_2O_3 CSNPs are shown in the Figure 5.1. In the XRD pattern of Fe_2O_3 NPs (Figure 5.1a), the major peaks are at 2θ = 33.23°, 35.50° and 54.00° corresponding to (104), (110) and (116) crystal planes and this diffraction pattern is well matched with JCPDS card number: (01-084-0307). The

XRD pattern of Gd_2O_3 NPs (Figure 5.1b) shows the existence of strong and sharp diffraction peaks at 2θ = 28.50°, 33.06°, 47.44° and 56.34° corresponding to its crystal planes are (222), (400), (440) and (622) respectively. The nature and position of the above diffraction peaks are characteristic of cubic Gd_2O_3 phase as cited in other reports [30] and JCPDS data (card number: 43-1014). The diffraction pattern of Fe_2O_3/Gd_2O_3 CSNPs (Figure 5.1c) shows the existence of diffraction peaks of both core and shell materials peak.

5.3.2 TEM Analyses

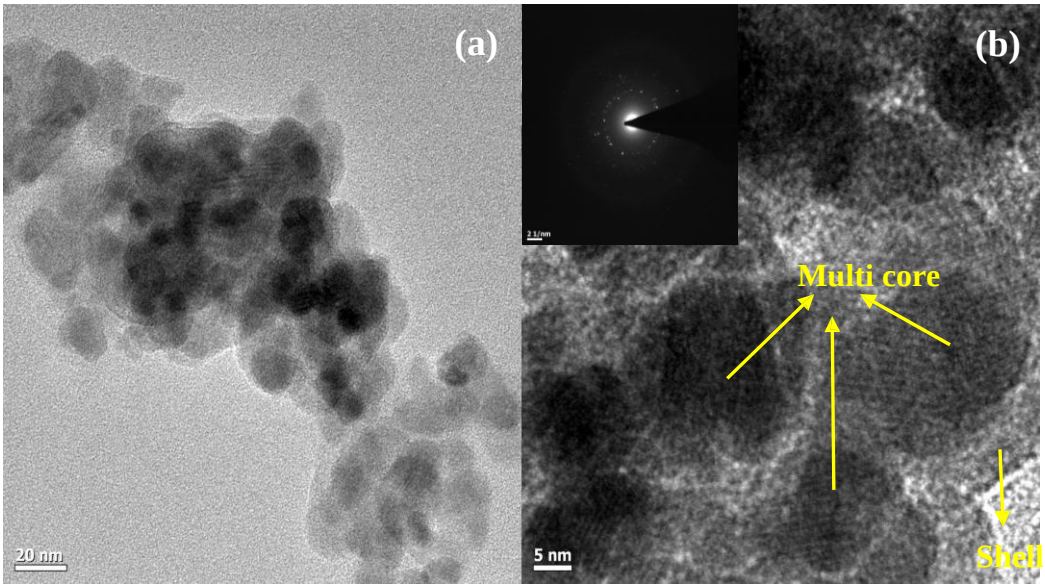

Figure 5.2 (a) TEM micrograph and (b) HRTEM micrograph of Fe_2O_3/Gd_2O_3 CSNPs. Inset Figure 5.2b shows SAED pattern of Fe_2O_3/Gd_2O_3 CSNP

The TEM micrograph of Fe_2O_3/Gd_2O_3 CSNPs is shown in Figure 5.2a, where the dark sphere of the multi core particles that are dispersed and encapsulated in the irregular continuous matrix is the Gd_2O_3 shell. The average core particle size is around ~ 15 nm and size of the CSNPs is found to be ~ 50nm. Figure 5.2b shows the high-resolution TEM micrograph which displays the visible lattice fringes and the core-shell morphology can be easily distinguished from this crystalline CSNPs. The

selected area electron diffraction (SAED) pattern shown in the inset of Figure 5.2b contains both ring and bright spot indicates the amorphous and crystalline nature of the sample.

5.3.3 AC Conductivity Studies

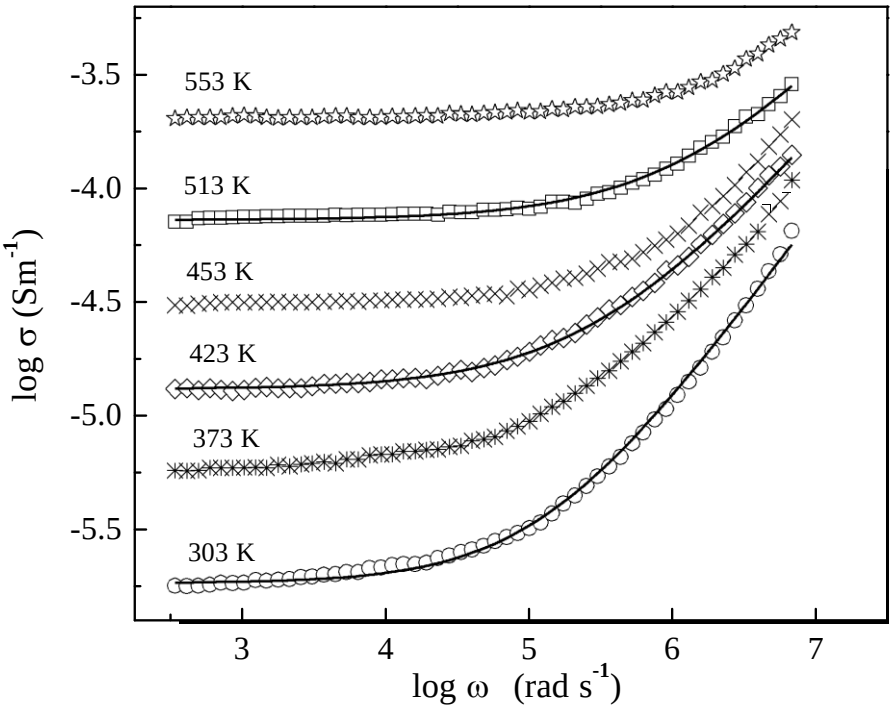

Figure 5.3 Frequency dependence of conductivity (σ) for Fe_2O_3/Gd_2O_3 CSNPs at various temperatures. Solid lines are the fitting of Jonscher‟s power law

The dielectric relaxation of insulating or semiconducting condensed matter system can be analysed in terms of dipolar and conductivity relaxation mechanisms. For dipolar relaxation originating from dipole motion, the dielectric response can be described as a direct relationship between the dielectric constant and the admittance (the reciprocal of the impedance). For conductivity relaxation, the dispersion of the dielectric constant is determined by a locally inhomogeneous potential barrier with long-range charge-carrier diffusion and the dielectric response can be described as a relationship between the electric modulus and the impedance. The relaxation time is determined by the reciprocal of the frequency where the maximum of the imaginary

part of the electric modulus or impedance is centered. Here, we have adopted the conductivity relaxation mechanism to investigate the dielectric relaxation phenomenon in Fe_2O_3/Gd_2O_3 CSNPs.

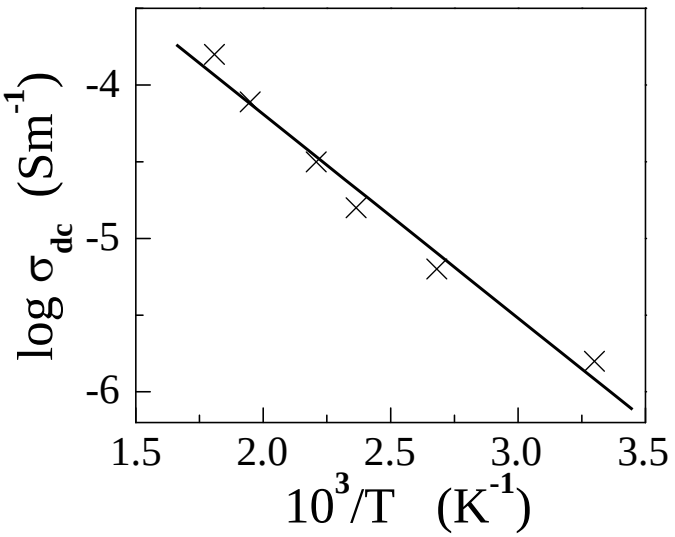

Figure 5.4 Arrhenius plot of dc conductivity for Fe_2O_3/Gd_2O_3 CSNPs

If one assumes that the total dielectric loss in the temperature range studied is due to conductivity, the appropriate formula for conductivity is $\zeta = \omega\varepsilon_0\varepsilon''$, here ζ is the real part of the conductivity. The frequency spectrum of conductivity for Fe_2O_3/Gd_2O_3 is shown in Figure 5.3 at different measuring temperatures. The conductivity shows dispersion. The value of ac conductivity decreases with decreasing frequency and becomes independent of frequency after a certain value. Extrapolation of this part to lower frequencies will give the dc conductivity (ζ_{dc}). The very basic fact about AC conductivity in Fe_2O_3/Gd_2O_3 is that ζ is an increasing function of frequency (any hopping model has this feature). In a hopping model, it is possible to distinguish different characteristic regions of frequency. At low frequencies where the conductivity is constant, the transport takes place on infinite paths. For a region of frequencies where the conductivity increases strongly with

frequency, the carriers can hop only between two sites and a total response is produced by the sum of the individual response of pairs of sites randomly distributed throughout the material. Frequency dependence of ac conductivity in this material is investigated by the power law relation as proposed by Jonscher [31]:

$$\sigma_1(\omega) = \sigma_o + A\omega^n \quad \text{..... (5.1)}$$

where the coefficient A and exponent n are temperature and material independent parameters. The term A on comprises ac dependence and characterises all dispersion phenomena. The experimental conductivity data are fitted with Eq. (5.1) and indicated by the solid lines in Figure 5.3. The values of n are found to be 0.86 – 0.7 for the temperature range 30 ^{o}C – 240 ^{o}C. The temperature dependence of ζ_{dc} obtained from the fitting of Eq. (5.1) follows the Arrhenius law as shown in the Figure 5.4. The activation energy as obtained from a linear fit of the experimental data is 0.26 eV. Such a value of activation energy corresponds to the hopping conduction mechanism in Fe_2O_3/Gd_2O_3 CSNPs.

5.3.4 Impedance Analysis

The angular frequency ω (=2πν) dependence of the real (*Z*′) and imaginary (*Z*″) parts of complex impedance for Fe_2O_3/Gd_2O_3 CSNPs at various temperatures is shown in Figure 5.5. It is evident from Figure 5.5b that the position of the relaxation peak in *Z*″ shifts to higher frequencies with increasing temperature and that a strong dispersion of *Z*″ exists. The total resistance decreases with an increase in temperature across the entire frequency range which shows the semiconducting behaviour of the material. It is clear that the width of the peaks in Figure 5.5b cannot be accounted for in terms of a mono-dispersive relaxation process, but points towards the possibility of a distribution of relaxation times. In order to account for it, Cole–Cole model is used to define the relaxation mechanism in this material and defined as [32]

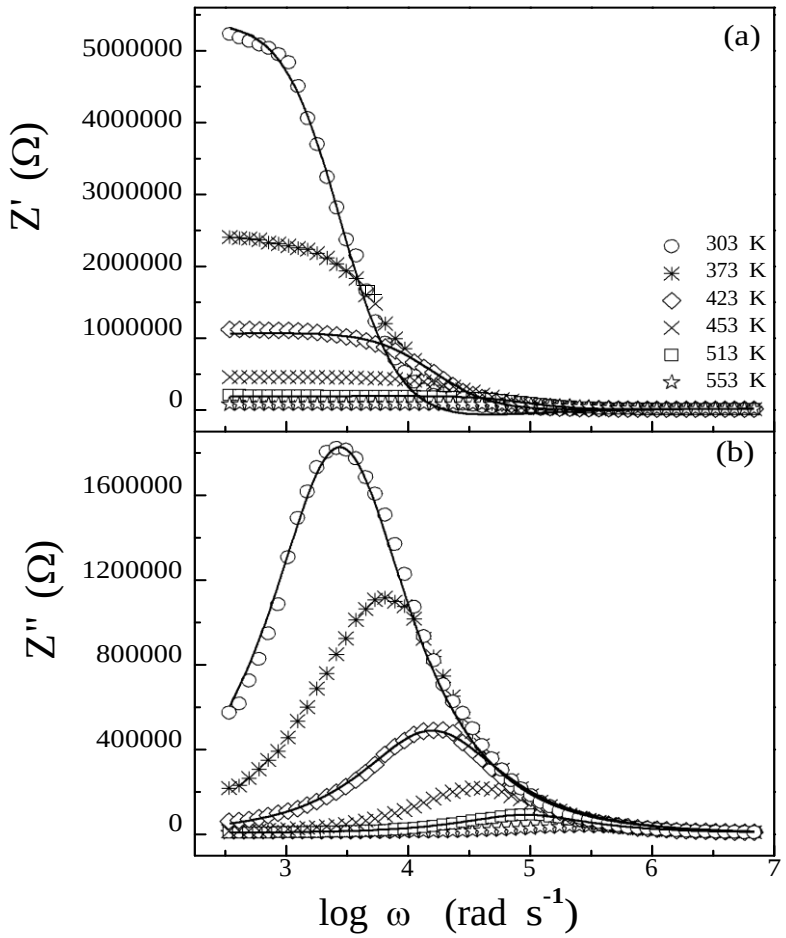

Figure 5.5 Frequency dependence of (a) Z' and (b) Z'' of Fe_2O_3/Gd_2O_3 CSNPs at various temperatures

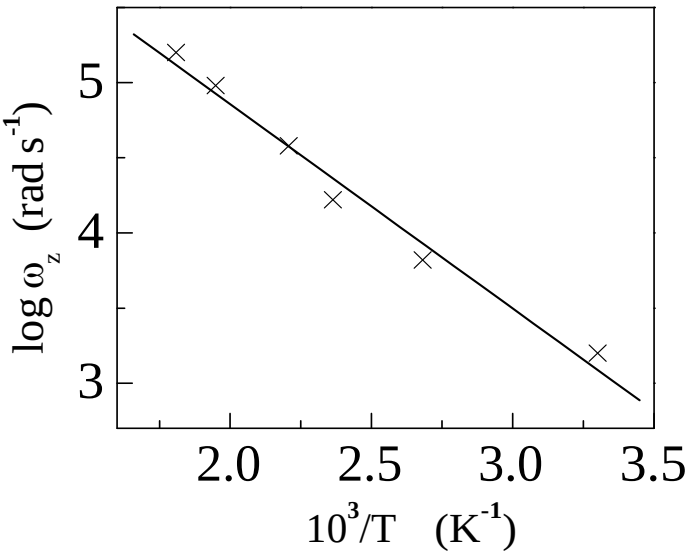

Figure 5.6 Arrhenius plot of ω_m for Z''max where the symbols are the experimental data points and the solid line is the least-squares straight-line fit

$$Z^* = R_\infty + \frac{R_0 - R_\infty}{1+(j\omega\tau_z)^\alpha} \qquad \text{.....(5.2)}$$

where R_0 and R_∞ are the resistances at very low and very high frequencies, respectively, ω_z (= $1/\eta_z$) is the characteristic relaxation frequency corresponding to the peak position of Z'' in the spectroscopic plot and α is a dimensionless exponent that denotes the angle of tilt of the circular arc from the real axis. The best fitting of the impedance data with Eq. (5.2) is shown by solid lines in Figure 5.5 for Z', Z'' and fitted data are listed in Table 5.1. The values of α indicate that the relaxation phenomenon in Fe_2O_3/Gd_2O_3 is polydispersive in nature (for monodispersive $\alpha = 0$). The activation energy as obtained from the linear fitting of the temperature dependence of ω_z (Figure 5.6) is found to be 0.27 eV.

Table 5.1 Fitting parameters of Equation (5.2)

Temperature (K)	**R_0-R_∞ (kΩ)**	**ω_m (kHz)**	α
303	2800	2.7	0.26
423	759	15.5	0.27
513	124	90	0.24

If we plot Z'' in scaled coordinates, i.e. Z''/Z''_m and log (ω/ω_z), the entire data collapse into one master curve as shown in the Figure 5.7. The scaling behaviour of Z'' clearly indicates that the dielectric relaxation in this material describes the same mechanism at various temperatures.

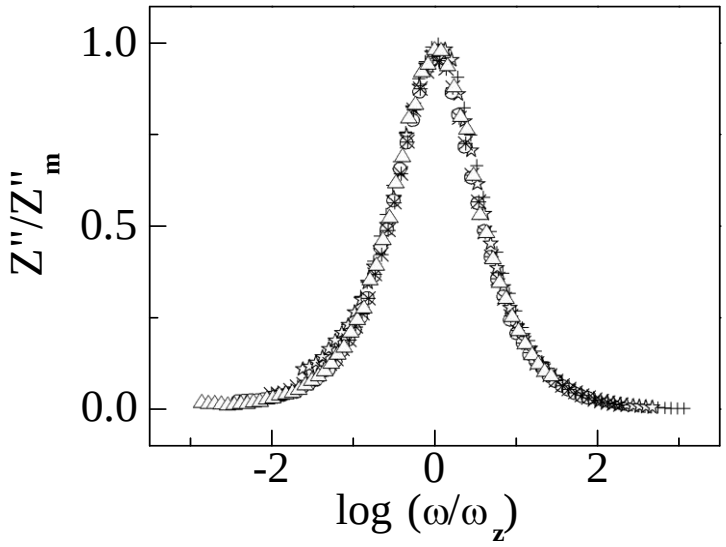

Figure 5.7 Scaling behaviour of *Z*″max at various temperatures for Fe_2O_3/Gd_2O_3 CSNPs

5.3.5 Electric Modulus

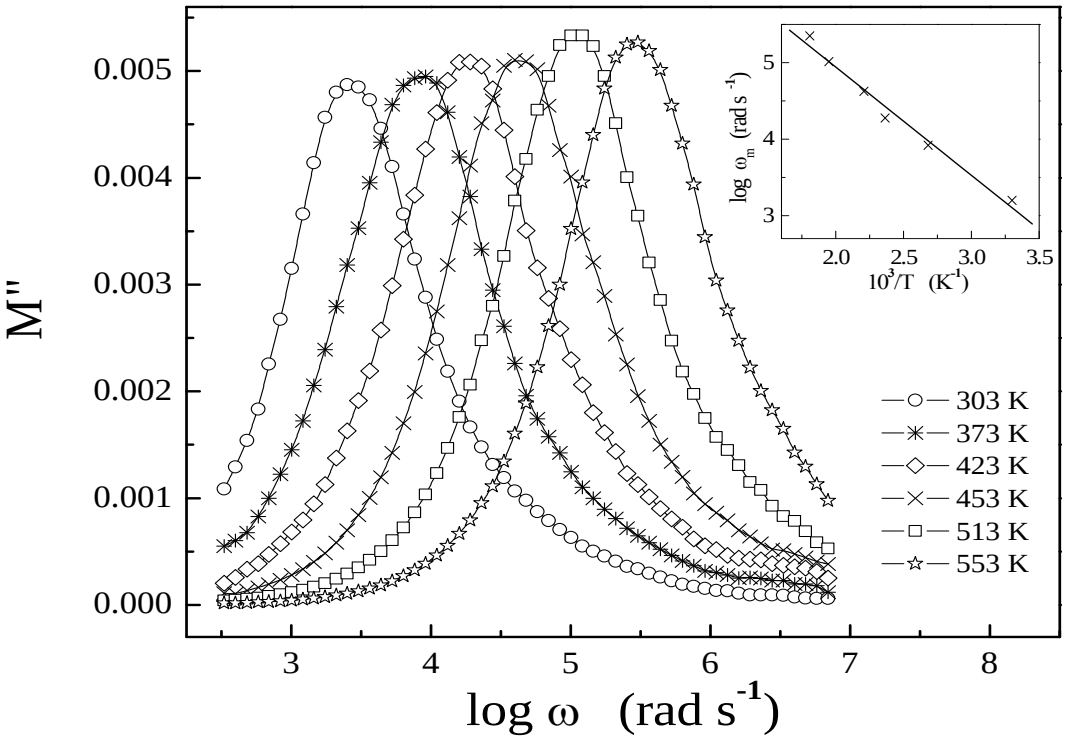

Figure 5.8 Frequency dependence of M″ for Fe_2O_3/Gd_2O_3 CSNPs at various temperatures. The Arrhenius plot of ω_m for M″ is shown in the inset where the symbols are the experimental points and the solid line is the least-squares straight-line fit

The electric modulus corresponds to the relaxation of the electric field in the materials when the electric displacement remains constant. Figure 5.8 displays the frequency (angular) dependence of M″ for Fe_2O_3/Gd_2O_3 as a function of temperature, where the relaxation peak moves towards lower frequencies during cooling of the sample. Consequently, it means that the relaxation rate for the process decreases with decrease in temperature. The peak height is inversely proportional to the capacitance of the sample. The temperature dependence of the frequency of maximum peak position in log ω *vs.* M″ plots follows the Arrhenius law as shown in the inset of Figure 5.8. The activation energy as obtained from the linear fit of the experimental data (inset of Figure 5.8) is found to be 0.28 eV which is nearly equal to the activation energy obtained from impedance formalism.

5.4 Conclusions

The Gd_2O_3 encapsulated Fe_2O_3 CSNPs have been synthesised by chemical method. The phase formation of the sample is confirmed by X-ray diffraction study. The core-shell morphology and average grain size of 60 nm is found by Transmission electron microscopy. The frequency-dependent dielectric dispersion of the material is investigated in the temperature range from 303 K to 553 K. The temperature dependent relaxation times are found to obey Arrhenius law having activation energy of 0.26 eV which indicates that the polaron hopping is responsible for conduction or dielectric relaxation in this material. The relaxation mechanism of these Fe_2O_3/Gd_2O_3 CSNPs has been discussed in the framework of conductivity and permittivity formalisms.

References

1. A. Roy, A. Parveen, R. Deshpande, R. Bhat and A. Koppalkar, J. Nanopart. Res. 15 (2013) 1337.
2. A. S. Lanje, S. J. Sharma, R. S. Ningthoujam, J.S. Ahn and R. B. Pode, Adv. Powder Technol. 24 (2013) 331.
3. N. Nakajima, M. Oki, Y. Isohama, H. Maruyama, Y. Tezuka, K. Ishiji, T. Iwazumi and K. Okada, Phys. Rev. B, 86 (2012) 224114 .
4. H. Yin, Z. Ma, M. Chi and S. Dai, Catal. Today, 160 (2011) 87.
5. F. X. Zhang, L. X. Dong, H. Huang, B. Lv, G. X. Zhu, P. J. Lei, S. Ma, W. Liu and D. Z. Zhang, Mater. Sci. Eng. A, 211 (2007) 454.
6. H. Shen, J. Yao and R. Gu, Trans. Nonferrous Met. Soc. China, 19 (2009) 652.
7. S. Xuan, J. X. Y. Wang, C. J. Yu and F. C. K. Leung, Langmuir, 25 (2009) 11835.
8. S. Balakrishnan, J. M. Bonder and C. G. Hadjipanayis, J. Magn. Magn. Mater. 321 (2009) 117.
9. F. Caruso, Adv. Mater. 13 (2001) 11.
10. C. M. Daniel and D. Astruc, Chem. Rev. 104 (2004) 293.
11. L. Qi, J. Ma, H. Cheng and Z. Zhao, Colloids Surf. A, 111 (1996) 195.
12. P. V. Kamat and B. Shanghavi, J. Phys. Chem. B, 101 (1997) 7675.
13. P. Scodeller, V. Flexer, R. Szamocki, J. E. Calvo, N. Tognalli, H. Trooani and A. Fainstein, J. Am. Chem. Soc. 130 (2008) 12690.
14. J. S. Oldenberg, D. R. Averitt, L. S. Westcott and N. Halas, J. Chem. Phys. Lett. 288 (1998) 243.
15. Z. Li, L. A. Fredin, P. Tewari, S. A. DiBenedetto, M. T. Lanagan, M. A. Ratner and T. J. Marks, Chem. Mater. 22 (2010) 5154.
16. T. I. Yang, R. N. C. Brown, L. C. Kempel and P. Kofinas, Nanotechnology, 22 (2011) 105601.
17. L. Xie, X. Huang, C. Wu and P. Jiang, J. Mater. Chem. 21 (2011) 5897.
18. X. F. Zhang, P. F. Guan and X. L. Dong, Appl. Phys. Lett. 96 (2010) 223111.
19. Y. Lin, L. Jiang, R. Zhao and C. W. Nan, Phys. Rev. B, 72 (2005) 014103.
20. D. R. Gulabshankar and S. V. Darshane, Bull. Chem. Soc. Jpn. 64 (1991) 2449.
21. V. G. G. Reddy, K. Sheela and V. S. Manorama, Int. J. Inorg. Mater. 2 (2000) 301.

22. K. Jung and C. Feldmann, J. Mater. Res. 15 (2000) 536.
23. T. S. Aruna, S. Gosh and C. K. Patil, Int. J. Inorg. Mater. 3 (2001) 387.
24. N. N. Mallikarjuna, S. K. Manohar, P. V. Kulkarni, A. Venkataraman and T. M. Aminabhavi, J. Appl. Polym. Sci. 97 (2005) 1868.
25. T. Wang, W. Li, L. Luo and Y. Zhu, Appl. Phys. Lett. 102 (2013) 092904.
26. J. Kwo, M. Hong, A. R. Kortan, K. T. Queeney, Y. J. Chabal, J. P. Mannaerts, T. Boone, J. J. Krajewski, A. M. Sergent and J. M. Rosamilia, Appl. Phys. Lett. 77 (2000) 130.
27. J. L. Bridot, A. C. Faure, S. Laurent, C. Riviere, C. Billotey, B. Hiba, M.Janier, V. Josserand, J. L. Coll, L. Vander Elst, R. Muller, S. Roux, P.Perriat and O. Tillement, J. Am. Chem. Soc. 129 (2007) 5076.
28. R. Bazzi, M. A. F. Gonzalez, C. Louis, K. Lebbou, C. Dujardin, A. Brenier, W. Zhang, O. Tillement, E. Bernstein and P. Perriat, J. Lumin. 445 (2003) 102.
29. J. C. Wang, C. S. Lai, Y. K. Chen, C. T. Lin, C. P. Liu, M. R. S. Huang and Y. C. Fang, Electrochem. Solid-State Lett. 12 (2009) H202.
30. T. K. Tseng, J. Choi, M. Davidson and P. H. Holloway, J. Mater. Chem. 20 (2010) 6115.
31. A. K. Jonscher, Dielectric Relaxation Solids, Chelsea Dielectrics Press, London, (1983).
32. K. S. Cole and R. H. Cole, J. Chem. Phys. 9 (1941) 341.